Model Predictive Control with Softened Constraints for Hybrid Electric Vehicle

Trieu Minh Vu*[a1], Reza Moezzi[b1], Klodian Dhoska[c3]

[1] Institute for Nanomaterials, Advanced Technologies and Innovation, Technical University of Liberec, Czechia

[2] Faculty of Mechatronics, Informatics and Interdisciplinary Studies, Technical University of Liberec, Czechia

[3] Department of Production and Management, Faculty of Mechanical Engineering, Polytechnic University of Tirana, Albania

*[a]trieu.minh.vu@tul.cz; [b]Reza.Moezzi@tul.cz; [c]kdhoska@fim.edu.al

ABSTRACT

This research work develops the modelling of a parallel hybrid electric vehicle (HEV) using a fully automated friction clutch connecting the combustion engine and the main electric motor to switch between the pure electric driving mode and the combustion engine driving mode. A new scheme of model predictive control (MPC) with softened constraints for this HEV is developed and applied to control the vehicle speed and torque of the motor and the combustion engine. The MPC scheme with softened constraints can provide better drivability and stability for the hybrid vehicle tracking on desired speeds and needed torques. This MPC can also change the driving modes with fast and smooth clutch engagement. The HEV can track better and faster along the desired speeds and torques amid the dynamic constraints imposed on the states, inputs and outputs. MPC with softened constraints can improve considerably the control system stability and robustness.

1. INTRODUCTION

In parallel hybrid electric vehicle, both combustion engine and main electric motor are installed in parallel and work in independent configuration. The vehicle can run and switch in four driving modes: pure main electric motor (EV1) at low speed and low load; pure combustion engine (EV2) at high speed and high load; both main electric motor and combustion engine (EV3) at very high and very high load; and all main electric motor, generator motor, and combustion engine (EV4) at extreme high load. In 2021, Hyundai has been introducing a new version of Sonata Hybrid series in [1], this middle size family passenger HEV combining update technologies for parallel electric vehicle as shown in Figure 1.
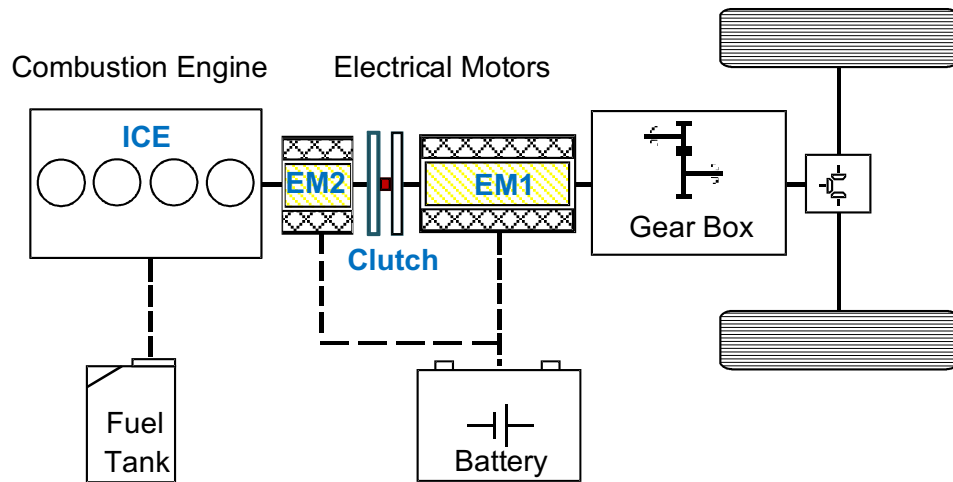
Figure 1. 2021 Hyundai Parallel HEV

This parallel HEV consists of one internal combustion engine (ICE) with four cylinders with multiple point injection, volume of 2.4 litters, max power of 156 kW at 6000 rpm, and the peak torque of 265 Nm; one electric motor starter (EM2) with max power of 8 kW and max torque of 43 Nm; the main electric motor (EM1) with max power of 35 kW and max torque of 205 Nm; the battery HEV Li-ion with capacity of 6.1 Ah; the transmission gear box with fully automated 6 speed and the friction clutch engagement. The vehicle curb weight is 1569 kg. This Sonata Hybrid vehicle is used to simulate our system modelling and test the new MPC scheme with softened constraints.

Controllers design for the HEV powertrains and speeds can be including model-free or model-based. Model-free controllers are mostly used with heuristic, fuzzy, neuro, AI, or human virtual and augmented reality. The use of model-free methods will be presented in the next part of this study. Model-based controllers can be used with conventional adaptive PID or H_2 or H_∞ or sliding mode control. But all conventional control methods cannot include the real-time dynamic constraints of the vehicle physical limits, the surrounding obstacles, and the environment (road and weather) conditions. Therefore, MPC with horizon and open loop control prediction subject to dynamic constraints are mainly used to control as real-time the HEV speeds and torques. Due to the limit size of this paper, we are reviewing some most recent research of MPC applications for HEV.

A recent modelling and control of dual clutch transmission for HEV are presented in [2] where a new controller is designed for synchronizing the dual clutch transmission (DCT) with higher performance and lower fuel consumption. Another MPC for autonomous driving vehicle is developed in [3] where the MPC is used to drive the HEV to track exactly given feasible trajectories. Also, a controller for hybrid dual-clutch transmission powertrain for HEV is introduced in [4] where the ICE and EM are driven by a DCT powertrain. A MPC for HEV with linear parameter and varying model is presented in [5] where the MPC controller is designed to improve the fuel economy of the power split HEV.

MPC for HEV is not only to control the torque and speed but also to control the gas emission and to improve the fuel economy. Authors in [6] develop a MPC with multi-objective function for HEVs for fuel economy, exhaust emission and collision detection

as well as to optimize the vehicle speed and engine torque. A new MPC design for HEV with adaptive cruise of autonomous electric vehicles is presented in [7]. A Hybrid MPC to optimize the HEV mode selection is introduced in [8] where the vehicle thermal management is controlled by this MPC subject to decision-making algorithms. Fuel economy and lower emission are also controlled by MPC with outer approximation and semi-convex cut generation and presented in [9].

Due to the recent world commitment to limit the increasement in global warming and to stop using fossil fuels, the plug-in and the pure electric vehicles are now expanding. MPC algorithms are also developed to control the plug-in hybrid vehicle (PHEV) as shown in [10]. In this study, a non-linear MPC is designed to control the torque-split and to optimize the fuel management. Authors in [11] also present a data-based scenario MPC framework to optimize the power consumption.

Nonlinear model predictive control (NMPC) has been widely used thank to the rapid increasement of computer capacity and speed. The computer now can calculate as real-time directly solution from very complex nonlinear functions. Therefore, authors in [12] provide MPC for nonlinear energy management of the power split HEV. Energy efficiency management for HEV is now also extended in communication among vehicles [13], in which, a MPC framework is proposed to generate the optimal torque and velocity by connecting the communication from vehicle-to-vehicle.

Authors in [14] review latest controllers from model-based in market on improving the energy management for HEV, where the MPC is used to calculate the optimal energy, torque and speed. Since MPC is one of the model-based algorithms, difficulty will be arising when there are existing mismatches between the model and the plant or the plant uncertainties. These mismatches and uncertainties may lead to the instability of the controller. Robust model predictive control (RMPC) algorithms are therefore, developed to deal to these uncertainties. Authors in [15] present a new method using matrix inequalities based RMPC for HEV considering external disturbances, time varying delays and model uncertainties. Authors in [16] introduce a real-time NMPC for the energy management of HEV using the sequential quadratic programming.

The use of MPC for pure electric vehicle is also referred in [17] for full battery consumption and road slope condition. Authors in [18] present a decentralized MPC of plug-in electric vehicles charging based on the alternative direction method of multipliers. Real-time MPC for HEV longitudinal tracking, jaw movement, dual-mode power split, and minimizing energy are presented in [19-22]. However, none of recent MPC methods is dealt with MPC with softened constraints. MPC is always subject to many strict constraints on states, outputs and inputs, therefore, it may not find out a feasible solution and it may become unstable. Since the MPC is a real-time optimizer, any failure solution cannot be tolerated. We propose to converse some physical strict constraints into softened constraints by adding some large penalty values into the objective function. This way can increase the stability and the robustness of the system dealing with uncertainties and initial conditions, that may that lead the outputs to violate constraints. Update new MPC calculations and advanced control techniques are referred to in references [23-32].

The layout of this paper is as followings: part 2 presents the modelling of parallel HEV; part 3 introduces the design of MPC; part 4 develops the MPC algorithms with softened constraints; part 5 illustrates simulations of MPC for HEV; and part 6 is conclusion.

2. MODELLING OF PARALLEL HEV

Schematic architecture of the 2021 Hyundai Sonata Hybrid in Figure 1 can be modelled with a simple drivetrain and shown in Figure 2. The first part of this mechanical structure consists of combustion engine ICE and the electric starter/generator motor EM2 can be grouped into one inertia J_1 including the left clutch disk, the shaft 1, EM2 and ICE. J_1 is modelled as one rigid inertia. M_{ICE} and M_{EV1} are the torques on ICE and EM2. θ_1 and ω_1 are the angular position and velocity of shaft 1. Similarly, J_2 is modelled as the lumped rigid inertia of the main electric motor EM1 and the right clutch disk, θ_2 and ω_2 are the angular position and velocity of shaft 2. The third powertrain part connecting the gearbox and the vehicle driven wheels can be modelled by a gear ratio i via a damper with k_θ, k_β, and k_α as the position, velocity, and acceleration damping coefficient. This third part consists of the lumped inertia J_3 of the rest of the vehicle including gearbox, differential gear, shaft 3 and the driven wheels. θ_3 and ω_3 are the angular position and velocity of shaft 3. And r is the vehicle wheel rolling radius.
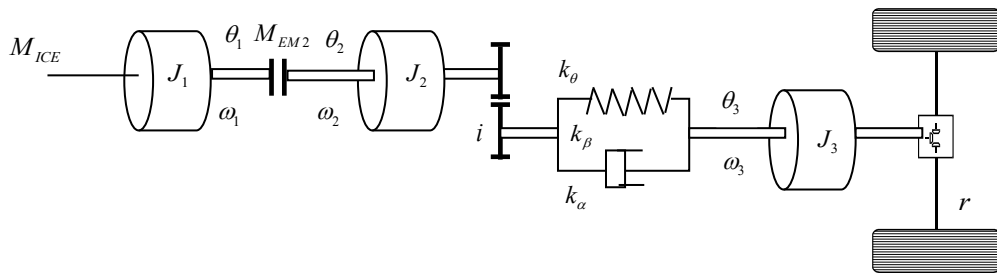

Figure 2. Simplified structure of parallel HEV

In this paper, vehicle dynamic formulas and constraints are referred to the technical book in [23]. The vehicle resistant torque is the approximation of the air density ρ, air drag coefficient c_w, the vehicle crossing area A, the wheel rolling radius r, vehicle friction resistant coefficient f_r, natural gravity g, vehicle mass m, and the polynomial coefficients of a_0, a_1, and a_2, correspondingly. The vehicle rolling resistance torque M_v can be calculated as:

$$M_v = \left(\frac{\rho}{2}c_w A(r\omega_3)^2 + f_r mg\right)r + a_0 + a_1\omega_3 + a_2\omega_3^2 \tag{1}$$

In equation (1), the additional road conditions such as the road dynamics and the road increasement and other environment conditions can be added as the disturbances leading to some reduction or increasement to the vehicle rolling resistance torque. Changes of vehicle velocity depending on the road conditions as well as the vehicle dynamic constraints between the vehicle speed and the vehicle steering wheel are referred in [23].

At low speed of less than 40 km/h, the clutch is open, only the main electric motor EM1 propels the HEV. The contribution of some other exponential coefficients is small

and can be ignored. The vehicle rolling resistance torque at low speed can be simplified as:

$$M_v = M_{v0} + k_v \omega_3 \tag{2}$$

where M_{v0} is the initial resistance constant of air drag and rolling friction, k_v is a linear coefficient depending on the gear ratio.

On the first part, the torque applied is:

$$M_{1o} = J_1 \dot{\omega}_1 \tag{3}$$

This torque can be calculated as:

$$M_{1o} = M_{ICE} + M_{M2} - M_C \tag{4}$$

where M_{ICE} is the torque from ICE, M_{M2} is the torque from motor ME2, and M_C is the torque from clutch.

When the clutch is locked, the clutch torque M_C is the maximum static friction,

$$M_C = M_{fmax}^{Static} = \frac{2}{3} r_C F_{NC} \mu_S \tag{6}$$

where r_C is the clutch radius, F_{NC} is the normal force, and μ_S is the clutch friction coefficient.

When the clutch is moving in transitional engagement, $M_C < M_{fmax}^{Static}$, the clutch torque is:

$$M_C = r_C F_{NC} sign(\omega_1 - \omega_2) \mu_R \tag{7}$$

where μ_R is the clutch slipping coefficient.

On the second part, the torque applied on the main motor ME1 is:

$$M_{2o} = k_\theta \theta_2 + \frac{k_\theta}{i} \theta_3 + k_v \omega_3 \tag{8}$$

The sum of inertias

$$M_{2o} = J_2 \dot{\omega}_2 i + J_3 \dot{\omega}_3 + k_v \omega_3 \tag{9}$$

And the torque velocity:

$$\dot{M}_{2o} = J_2 \ddot{\omega}_2 i + k_\alpha \left(\frac{\dot{\omega}_2}{i} - \dot{\omega}_3\right) + k_\beta \left(\frac{\omega_2}{i} - \omega_3\right) \tag{10}$$

The balance of torque M_{2o} is:

$$M_{2o} = (M_{EM2} + M_c)\eta i - M_{v0} \tag{11}$$

with η is the transmission efficiency of the gearbox and the differential gear.

The angular acceleration of the shaft 1:

$$\dot{\omega}_1 = -\frac{k_{\beta 1} \omega_1}{J_1} + \frac{M_{ICE}}{J_1} + \frac{M_{M1}}{J_1} + \frac{-M_C}{J_1} \tag{12}$$

where $k_{\beta 1}$ is the shaft 1 friction coefficient.

The angular acceleration of the shaft 2:

$$\dot{\omega}_2 = -\frac{k_{\beta 2}\omega_3}{J_2 i} - \frac{J_3 \dot{\omega}_3}{J_2 i} - \frac{\eta M_{M2}}{J_2} + \frac{\eta M_C}{J_2} - \frac{M_{v0}}{J_2 i} \tag{13}$$

where $k_{\beta 2}$ is the shaft 2 friction coefficient.

And finally, the angular acceleration of the shaft 3 is:

$$\dot{\omega}_3 = \frac{k_{\beta 3}\omega_3}{J_3} + M_{v0} \tag{14}$$

where $k_{\beta 3}$ is the shaft 3 friction coefficient.

The jerk on the drivetrain is:

$$\ddot{\omega}_3 = \frac{k_{\beta 2}\omega_2}{J_3 i} - \frac{(k_{\beta 2}J_2 i^2 + k_\alpha k_v)\omega_3}{J_2 J_3 i^2} - \left(\frac{k_v + k_\alpha}{J_3} + \frac{k_\alpha}{J_2 i^2}\right)\dot{\omega}_3 + \frac{k_\alpha \eta(M_{M2} + M_C)}{J_2 J_3 i} - \frac{k_\alpha M_{v0}}{J_2 J_3 i^2} \tag{15}$$

The torque generated on the main motor is:

$$M_{DC\_MOTOR} = \frac{k_T}{R_I}V - \frac{k_E k_T}{R_I}\omega \tag{16}$$

where M_{DC_MOTOR} is the main motor torque, k_T is the motor constant, $k_T = \frac{M_{Torque}}{I_{Current}}$ (Nm/A); k_E is the electromotive force (EMF) constant, $k_E = k_T$, R_I is the resistance, V is the voltage supply, and ω is the angular velocity.

Now we process and transform all above equations into a first order linear system as:

$$\dot{\theta}_1 = [0 + \quad \omega_1 + \quad 0 + \quad 0 + \quad 0 + \quad 0 + \quad 0] + [0 + \quad 0 + \quad 0 + \quad 0 + \quad 0] \tag{17}$$

$$= \left[0 + \quad \frac{-\left(k_{\beta 1} + \frac{k_{E1}k_{T1}}{R_{I1}}\right)\omega_1}{J_1} + \quad 0 + \quad 0 + \quad 0 + \quad 0 + \quad 0\right] + \left[\frac{M_{ICE}}{J_1} + \quad \frac{k_{T1}V_1}{R_{I1}J_1} + \quad 0 + \quad \frac{-M_C}{J_1} + \quad 0\right] \tag{18}$$

$$\dot{\theta}_1 = [0 + \quad \omega_1 + \quad 0 + \quad 0 + \quad 0 + \quad 0 + \quad 0] + [0 + \quad 0 + \quad 0 + \quad 0 + \quad 0] \tag{19}$$

$$\dot{\omega}_2 = \left[0 + \quad 0 + \quad 0 + \quad 0 + \quad 0 + \quad \frac{-\left(k_{\beta 2} + \frac{k_{E2}k_{T2}}{R_{I2}}\right)\omega_3}{J_2 i} + \quad \frac{-J_3 \dot{\omega}_3}{J_2 i}\right]$$
$$+ \left[0 + \quad 0 + \quad \frac{-\eta k_{T2}V_2}{R_{I2}J_2} + \quad \frac{\eta M_C}{J_2} + \quad \frac{-M_{v0}}{J_2 i}\right] \tag{20}$$

$$\dot{\theta}_3 = [0 + \quad 0 + \quad 0 + \quad 0 + \quad 0 + \quad \omega_3 + \quad 0] + [0 + \quad 0 + \quad 0 + \quad 0 + \quad 0] \tag{21}$$

$$\dot{\omega}_3 = \left[0 + \quad 0 + \quad 0 + \quad 0 + \quad 0 + \quad \frac{k_{\beta 3}\omega_3}{J_3} + \quad 0\right] + [0 + \quad 0 + \quad 0 + \quad 0 + \quad M_{v0}] \tag{22}$$

$$\ddot{\omega}_3 = \left[0+ \quad 0+ \quad 0+ \quad \frac{-\left(k_{\beta2}+\dfrac{k_{E2}k_{T2}}{R_{I2}}\right)\omega_2}{J_3 i} + \quad 0+ \quad \frac{-\left(k_{\beta2}J_2 i^2 + k_\alpha k_v\right)\omega_3}{J_2 J_3 i^2} + \quad -\left(\frac{k_v+k_\alpha}{J_3}+\frac{k_\alpha}{J_2 i^2}\right)\dot{\omega}_3 \right] \quad (23)$$

$$+\left[0+ \quad 0+ \quad \frac{-k_\alpha \eta k_{T2} V_2}{R_{I2} J_2 J_3 i} + \frac{k_\alpha \eta M_C}{J_2 J_3 i} + \frac{-k_\alpha M_{v0}}{J_2 J_3 i^2} \right]$$

If we put the space vector $x_0 = [\theta_1 \quad \omega_1 \quad \theta_2 \quad \omega_2 \quad \theta_2 \quad \omega_3 \quad \dot{\omega}_3]'$, and the input vector as $u_0 = [M_{ICE} \quad V_1 \quad V_2 \quad M_C \quad M_{v0}]'$ for the torque on the combustion engine ICE, the input voltage for motor EM1 and EM2, torque on clutch, and the initial air-drag load, a linear space state of the vehicle dynamics system can be formed as:

$$\dot{x}_0 = \begin{bmatrix}
0 & 1 & 0 & 0 & 0 & 0 & 0 \\
0 & \dfrac{-\left(k_{\beta1}+\dfrac{k_{E1}k_{T1}}{R_1}\right)}{J_1} & 0 & 0 & 0 & 0 & 0 \\
0 & 0 & 0 & 1 & 0 & 0 & 0 \\
0 & 0 & 0 & 0 & 0 & \dfrac{-\left(k_{\beta2}+\dfrac{k_{E2}k_{T2}}{R_2}\right)}{J_2 i} & \dfrac{-J_3 \dot{\omega}_3}{J_2 i} \\
0 & 0 & 0 & 0 & 0 & 1 & 0 \\
0 & 0 & 0 & 0 & 0 & \dfrac{k_{\beta3}\omega_3}{J_3} & 0 \\
0 & 0 & 0 & \dfrac{-\left(k_{\beta2}+\dfrac{k_{E2}k_{T2}}{R_2}\right)}{J_3 i} & 0 & \dfrac{-\left(k_{\beta2}J_2 i^2 + k_\alpha k_v\right)}{J_2 J_3 i^2} & -\left(\dfrac{k_v+k_\alpha}{J_3}+\dfrac{k_\alpha}{J_2 i^2}\right)
\end{bmatrix} x_0$$

$$+ \begin{bmatrix}
0 & 0 & 0 & 0 & 0 \\
\dfrac{1}{J_1} & \dfrac{k_{T1}}{R_1 J_1} & 0 & \dfrac{-1}{J_1} & 0 \\
0 & 0 & 0 & 0 & 0 \\
0 & 0 & \dfrac{\eta k_{T2}}{R_2 J_2} & \dfrac{\eta}{J_2} & \dfrac{-1}{J_2 i} \\
0 & 0 & 0 & 0 & 0 \\
0 & 0 & 0 & 0 & 1 \\
0 & 0 & \dfrac{k_\alpha \eta k_{T2}}{R_2 J_2 J_3 i} & \dfrac{k_\alpha \eta}{J_2 J_3 i} & \dfrac{-k_\alpha}{J_2 J_3 i^2}
\end{bmatrix} u_0 \qquad (24)$$

The linear first order state space model in (24) can be used to create the MPC algorithms in the next part. System in (24) is including the acceleration $\dot{\omega}_3$ and jerk $\ddot{\omega}_3$, which can be used to simulate and regulate the HEV driving comfortability.

When the HEV runs in low speed less than 40km/h, only the main motor EM1 is working. The inputs of $M_{ICE} = 0$, $V_1 = 0$, $M_C = 0$. The state variables of $\theta_1 = 0$, $\omega_1 = 0$. Then, the above linear system can be simplified as:

$$\begin{cases} \dot{x}_p = A_p x_p + B_p u_p \\ y_p = C_p x_p + D_p u_p \end{cases}$$

$$A_p = \begin{bmatrix} 0 & 1 & 0 & 0 \\ 0 & -\dfrac{k_{\beta2} + \dfrac{k_{E2} k_{T2}}{R_{I2}}}{J_2} & 0 & 0 \\ 0 & 0 & 0 & 1 \\ 0 & 0 & 0 & -\dfrac{(k_{\beta3} - k_v)}{J_3} \end{bmatrix}, \quad B_p = \begin{bmatrix} 0 & 0 \\ \dfrac{k_{T2}}{R_{I2} J_2} & 0 \\ 0 & 0 \\ 0 & -1 \end{bmatrix} \tag{25}$$

$$C_p = \begin{bmatrix} 0 & 0 & 0 & 1 \\ k_\theta & 0 & \dfrac{k_\theta}{i} & 0 \end{bmatrix}; \quad D_p = \begin{bmatrix} 0 & 0 \\ 0 & 1 \end{bmatrix}$$

where the states $x_p = [\theta_2 \ \omega_2 \ \theta_3 \ \omega_3]'$, inputs $u_p = [V_2 \ M_{v0}]'$, outputs $y_p = [\omega_3 \ T_{Torque3}]'$. The output $T_{Torque3}$ is the unmeasured torque at shaft 3. In this equation, k_θ is the torsional rigidity, $k_\theta = \dfrac{M_{Torque}}{\varphi} = \dfrac{GJ}{l}$, and φ is the twist angle, $\varphi = \theta_2 - \dfrac{\theta_3}{i}$. G is the rigidity modulus. l is the shaft length. And J is the lumped inertia moment, $J = J_2 + J_3$.

When the HEV runs in high speed greater than 40 km/h, the starter motor EM2 activates the combustion engine ICE while the friction clutch is still open, the state equations of the first part can be written as:

$$\dot{\theta}_1 = [0 + \quad \omega_1] + [0 + \quad 0] \tag{26}$$

$$\dot{\omega}_1 = \begin{bmatrix} 0 & -\dfrac{\left(k_{\beta1} + \dfrac{k_{E1} k_{T1}}{R_{I1}}\right)}{J_1} \end{bmatrix} \omega_1 + \begin{bmatrix} \dfrac{\varsigma k_{T1}}{R_{I1} J_1} V_1 + \dfrac{1}{J_1} M_{ICE} \end{bmatrix} \tag{27}$$

where ς is the additional coefficient for starting motor EM2 as a compensation load for the starting period. The linear state space system in the first part is:

$$\begin{cases} \dot{x}_e = A_e x_e + B_e u_e \\ y_e = C_e x_e + D_e u_e \end{cases}$$

$$A_e = \begin{bmatrix} 0 & 1 \\ 0 & -\dfrac{\left(k_{\beta1} + \dfrac{k_{T1}^2}{R_{I1}}\right)}{J_1} \end{bmatrix}; \quad B_e = \begin{bmatrix} 0 & 0 \\ \dfrac{\varsigma k_{T1}}{R_{I1} J_1} & \dfrac{1}{J_1} \end{bmatrix}; C_e = \begin{bmatrix} 0 & 1 \\ 0 & \dfrac{\left(k_{\beta1} + \dfrac{k_{E1} k_{T1}}{R_1}\right)}{J_1} \end{bmatrix}; \tag{28}$$

$$D_e = \begin{bmatrix} 0 & 0 \\ 0 & 0 \end{bmatrix}$$

where $x_e = [\theta_1 \ \omega_1]'$, $u_e = [V_1 \ M_{ICE}]'$, $y_e = [\omega_1 \ T_{Torque1}]'$. The output $T_{Torque1}$ is the unmeasured torque at shaft 1.

3. MODEL PREDICTIVE CONTROL FOR HEV

MPC is an open loop, infinite horizon prediction and optimization controller subject to dynamic constraints. The continuous first order linear space state equation in (24) can be discretized into time interval with discrete k and $k + 1 = k + \Delta t$, Δt is the computer

scanning speed or the time sampling interval. Now the continuous time form in (24) can be discretized into:

$$\begin{cases} x_{t+1} = Ax_t + Bu_t \\ y_t = Cx_t + Du_t \end{cases} \tag{29}$$

Subject to the states, inputs, outputs and the inputs increasement constraints

$$x_k \in X, \; u_k \in U, \; \Delta u_t = u_t - u_{t-1} \in \Delta U, \text{ and } y_k \in Y \tag{30}$$

MPC calculates the open loop input and output prediction horizon, for the calculation simplicity, we assume the input prediction length is always equal to the output prediction length or $N_u = N_y$. The objective function of the MPC for HEV is:

$$\min_{U \triangleq \{\Delta u_1, \dots, \Delta u_{1+N_u-1}\}} \left\{ J(U, x(t)) = \sum_{k=0}^{N_y-1} \left[(y_{t+k|t} - r)'Q(y_{t+k|t} - r) + \Delta u'_{t+k} R \Delta u_{t+k} \right] \right\} \tag{31}$$

subject to (30) as $u_k \in U$, and $u_{k+i} \in [umax_{min}]$, $\Delta u_{k+i} \in [\Delta umax_{min}]$, for $i = 0,1,\dots,N_u - 1$, $y_k \in Y$, and $y_{k+i|k} \in [ymax_{min}]$, for $i = 0,1,\dots,N_y - 1$, $\Delta u_k = u_k - u_{k-1} \in \Delta U$, and $\Delta u_{k+i} = 0$, for $i \geq N_u$, $x_{k|k} = x(k)$, $x_{k+i+1|k} = A(k)x_{k+i|k} + B(k)u_{k+i}$, $u_{k+i|k} = u_{k+i-1|k} + \Delta u_{k+i|k}$, $y_{k+i|k} = C(k)x_{k+i|k}$, where $x(k)$ is the state variables, $U \triangleq \{\Delta u_k, \dots, \Delta u_{k+N_u-1}\}$ is the solution of predictive input from k to N_u. And N_y is the predictive output $y_{k+i|k}$, $r_{k+i|k}$ is the desired speed setpoints; $\Delta u_{k+i|k}$ is the input predictive increments, $\Delta u_{k+i|k} = u_{k+i|k} - u_{k+i-1|k}$; $Q = Q' \geq 0$, and $R = R' > 0$ are the weighting matrices for the outputs and the inputs, respectively.

By substituting $x_{k+j|k} = A^k x(k) + \sum_{j=0}^{k-1} A^j B u_{k+j-1-j}$, equation (31) can be transformed as

$$V(x(k)) = \frac{1}{2} x'(k)Yx(k) + \min_U \left\{ \frac{1}{2} U'HU + x'(k)FU \right\}, \tag{32}$$

subject to the linear matrices' inequality, $GU \leq W + Ex(t)$, where the column vector $U \triangleq [u'_k, \dots, u'_{k+N-1}] \in \mathbb{R}^s$, $s \triangleq mN_u$ is the optimization vector, $H = H' > 0$, and $H,$ F, Y, G, W, E are obtained from Q, R and in (31) as only the optimizer vector U is needed, the term involving Y is usually removed from (32). The optimization problem (31) is a quadratic program (QP). The MPC optimizer will calculate the optimal input vector $U \triangleq \{\Delta u_k, \dots, \Delta u_{k+N_u-1}\}$ subject to the dynamic constraints of the inputs, $u_k \in U$, and $u_{k+i} \in [umax_{min}]$; of the outputs $y_k \in Y$, and $y_{k+i|k} \in [ymax_{min}]$; and of the input increments $\Delta u_{k+i} \in [\Delta umax_{min}]$. But only the first input increment, Δu_k, is inserted into the implementation. Then, the optimizer will update the outputs and states variables and repeat the calculation.

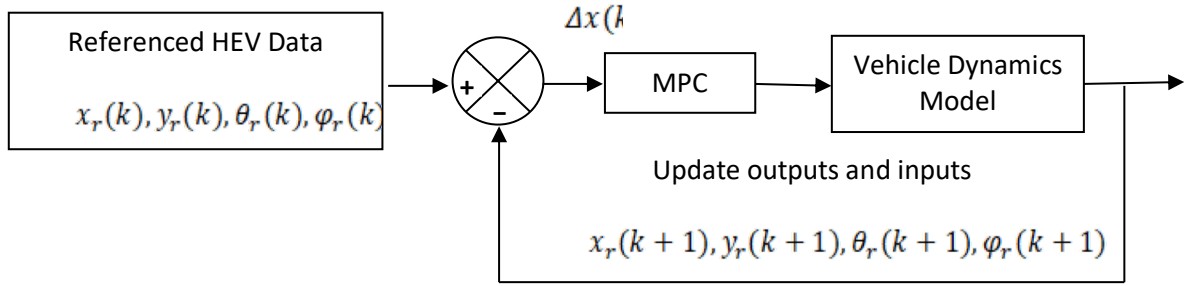A diagram of the MPC for HEV is drawn in Figure 3.

Figure 3. MPC diagram system

The MPC scheme for HEV in Figure 3 calculates the real-time optimal control action, $\Delta u(k)$, and feeds into the vehicle dynamic equations and update the current states, inputs and outputs. The update states, inputs and outputs will feedback and compare to the reference desired trajectory data for generating the next optimal control action $\Delta u(k)$ in the next interval.

When the system is nonlinear and has the general derivative nonlinear from as:

$$\dot{X} = f(x, u) \tag{33}$$

where x is the state variables and u is the inputs. The nonlinear equation in (33) can be approximated in a Taylor series at referenced positions of (x_r, u_r) for $\dot{X}_r = f(x_r, u_r)$, that:

$$\dot{X} \approx f(x_r, u_r) + f_{x,r}(x - x_r) + f_{u,r}(u - u_r) \tag{34}$$

in which, $f_{x,r}$ and $f_{r,x}$ are the Jacobean function of x and u, moving around the referenced positions (x_r, u_r).

Subtraction (34) for $\dot{X}_r = f(x_r, u_r)$, we can obtain an approximation linear form in continuous time (t):

$$\dot{\tilde{X}}(t) = A(t)\tilde{X}(t) + B(t)\tilde{u}(t) \tag{35}$$

The linearized system in (35) can be used as the linear system in (24) for the MPC calculation. However, the MPC real-time optimal control action $\Delta u(k)$ must be fed into the original nonlinear system in (33) for the update states, outputs, and inputs.

4. MPC WITH SOFTENED CONSTRAINTS FOR HEV

The conventional MPC objective function in (31) subject to the constraints in (30) on states, outputs, inputs and input increasement may deal with so many hard constraints. The MPC optimizer may not find out solution satisfying all constraints. So that we now consider to widen the MPC feasibility by converting some possible hard constraints from (30) into softened constraints to increase the possibility to find out solution. The new MPC scheme subject to softened constraints has the following form:

$$\min_{U \triangleq \{\Delta u_k, \ldots, \Delta u_{k+N_u-1}\}} \left\{ J(U, x(k)) \right.$$

$$= \sum_{i=0}^{N_y-1} \left[(y_{k+i|k} - r_{k+i|k})'Q(y_{k+i|k} - r_{k+i|k}) + \Delta u'_{k+i|k} R \Delta u_{k+i|k} \right. \tag{36}$$

$$\left. + \varepsilon_i'(k)\Lambda\varepsilon_i(k) + 2\mu'\varepsilon_{k+i|k} \right] \right\}$$

subject to

$$\begin{bmatrix} 1 & z_i' \\ z_i & X + \mu\varepsilon_i I \end{bmatrix} \geq 0 \tag{37}$$

$$\begin{cases} \min_j X_{jj} \leq x_{max}^2 \\ \forall z_i \in vert\left\{ \chi_{u^*(\cdot|k)}^{k+i|k}(x(k)) \right\}, \forall i \in \{1, \ldots, N\} \end{cases}$$

where μ is assigned as big values as a weighting factor ($\mu > 0$), and ε_i is the constraints penalty terms ($\varepsilon_i \geq 0$) added into the MPC objective function. X and z_i are the corresponding matrix of the hard constraints.

The new items in (37) are softened constraints selected from hard constraints in $u_k \in \mathcal{U}$, and $u_{k+i} \in [umax_{min}]$, $\Delta u_{k+i} \in [\Delta umax_{min}]$, for $i = 0,1, \ldots, N_u - 1$, $y_k \in \mathcal{Y}$, and $y_{k+i|k} \in [ymax_{min}]$, for $i = 0,1, \ldots, N_y - 1$, $\Delta u_k = u_k - u_{k-1} \in \Delta\mathcal{U}$, and $\Delta u_{k+i} = 0$, for $i \geq N_u$, $x_{k|k} = x(k)$, $x_{k+i+1|k} = A(k)x_{k+i|k} + B(k)u_{k+i}$, $u_{k+i|k} = u_{k+i-1|k} + \Delta u_{k+i|k}$, $y_{k+i|k} = C(k)x_{k+i|k}$, where, $\varepsilon_i(k) = [\varepsilon_y; \varepsilon_u]$, $y_{k+i|k} y_{max_{min}}$ and $u_{k+i|k} u_{max_{min}}$; and $\Lambda = \Lambda' \geq 0$ is the additional penalty matrix (generally $\Lambda > 0$ and assign to small values); In this new MPC scheme, the penalty term of softened constraints $\sum_{i=0}^{N_p} \left[\varepsilon'_{k+i|k}\Lambda\varepsilon_{k+i|k} + 2\mu'\varepsilon_{k+i|k} \right]$ is added into the objective function with positive definite and symmetric matrix Λ; This term penalizes violations of constraints and when possible, the free constrained solution will be returned.

Now this MPC calculates the new optimization vector $U_S = \begin{bmatrix} U \\ \varepsilon \end{bmatrix}$ and the new MPC computational algorithms will be:

$$\Psi_S(x(t)) = \min_{U_S} \left\{ \frac{1}{2} U_S' H_S U_S + x'(t) F_S U_S \right\}, \tag{38}$$

subject to $G_S U_S \leq W_S + E_S x(k)$,

where $U_S \triangleq \left[u'_k, u'_{k+1}, \ldots, u'_{k+N_p-1}, \varepsilon'_k, \varepsilon'_{k+1}, \ldots, \varepsilon'_{k+N_p} \right]'$ is the new optimization input vector, $H_S = \begin{bmatrix} H & 0 \\ 0 & M \end{bmatrix}$ and $F_S = [F \quad \mu]$, and matrices for inequality constraints H, F, G, W, and E are obtained from equation (38),

$$G_S = \begin{bmatrix} G & 0 \\ g_S & -I \\ 0 & -I \end{bmatrix} \text{ with } g_S = \begin{bmatrix} 0 & 0 & 0 & \cdots & 0 \\ ZB & 0 & 0 & \cdots & 0 \\ ZAB & ZB & 0 & \cdots & 0 \\ \cdots & & \ddots & \ddots & \vdots \\ ZA^{N_p-1}B & ZA^{N_p-2}B & \cdots & \cdots & ZB \end{bmatrix},$$

$$W_S = \begin{bmatrix} W \\ w_S \\ 0 \end{bmatrix} \text{ with } w_S = \begin{bmatrix} Z \\ \vdots \\ Z \end{bmatrix}, \text{ and } E_S = \begin{bmatrix} E \\ e_S \\ 0 \end{bmatrix} \text{ with } e_S = \begin{bmatrix} -Z \\ -ZA \\ -ZA^2 \\ \vdots \\ -ZA^{N_p} \end{bmatrix}.$$

To illustrate the ability of this controller, we test the two MPC schemes in (31) and in (36) by the following simple example as considering the below nonlinear system:

$$\dot{x}_1 = 2x_2 + u(1 + x_1)$$
$$\dot{x}_2 = 2x_1 + u(1 - 3x_2)$$

(39)

It is assumed that the system in (39) is subjected to the hard state and input constraints $x_{min} = \begin{bmatrix} -1 \\ -1 \end{bmatrix}$ and $-2 \le u \le 2$. The linearized approximation of this system in (35) is: $\dot{x} = Ax + Bu$, in which, $A = \begin{bmatrix} 0 & 2 \\ 2 & 0 \end{bmatrix}$ and $B = \begin{bmatrix} 1 \\ 1 \end{bmatrix}$. The weighting matrices are chosen as $Q = \begin{bmatrix} 1 & 0 \\ 0 & 1 \end{bmatrix}$ and $R = 1$. The weighting matrices for softened constraints are chosen as $\Lambda = \begin{bmatrix} 1 & 0 \\ 0 & 1 \end{bmatrix}$ and $\mu = 10{,}000$. It is assumed that the system is starting form an initial state position, $x_0 = \begin{bmatrix} -0.72 \\ -0.35 \end{bmatrix}$. Figure 4 shows the performances of two NMPC schemes: This initial state position x_0 does not lead to any violation of states and input ($x_{min} = \begin{bmatrix} -1 \\ -1 \end{bmatrix}$ and $-2 \le u \le 2$). In this x_0, the solutions of the two control schemes are always available. We can see that, the NMPC with softened state approaches the asymptotic point faster than the hard constraints. It means that, if we loosen somehow some constraints, the optimizer can generate easier optimal inputs and the system will be more stable.

It is interesting to see in Figure 4 that, both schemes have $x_{1\,min}^{Hard} = -0.8475$ and $x_{1\,min}^{Softened} = -0.8483$, almost reach the hard constraint of $x_{min} = \begin{bmatrix} -1 \\ -1 \end{bmatrix}$. These states still have not violated the state constraints but if we select some other initial positions x_0, that may lead to some state and input violations.

Now, if we select $x_0 = \begin{bmatrix} -0.9 \\ -0.8 \end{bmatrix}$, this initial condition will lead to the violations of the state and the input constraints as $x_{1\,min} = -1.0441$ and $u_{max} = 2.2303$. These violations will make the RMPC with hard constraints infeasible. Meanwhile, the RMPC scheme with softened constraints is still running well and still easily to find out optimal input solutions as shown in Figure 5. And after a very short transitional period, the fully constrained solution is returned or there is no more constrained violation.
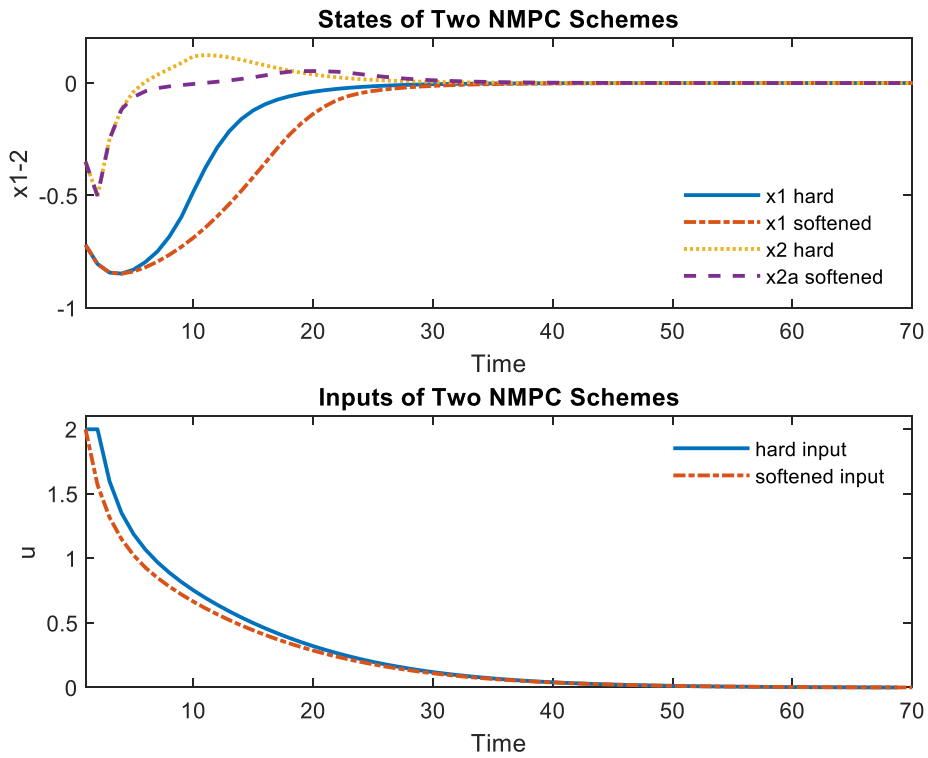
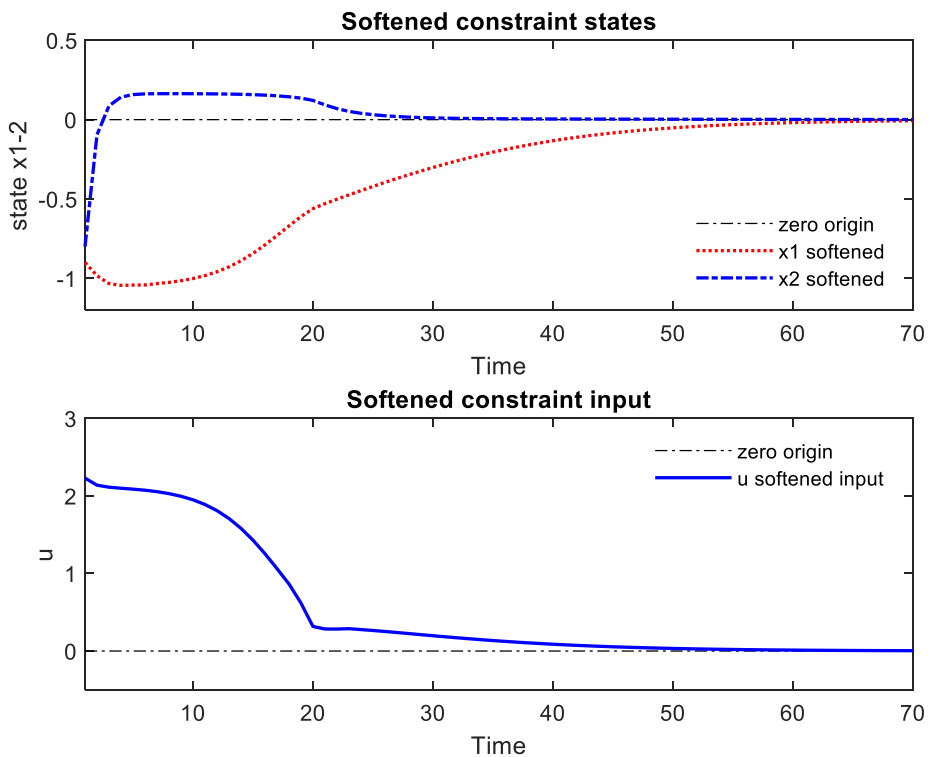Figure 4. Performance of two NMPC schemes

Figure 5. Softened Constraint NMPC

The new MPC scheme with softened constraints for HEV will be further analysed and simulated in the next part.

5. MPC WITH SOFTENED CONSTRAINTS FOR HEV

5.1 MPC for HEV in pure electrical drive

The main motor ME1 is used to run the HEV in low speed. In this mode, the clutch is open. ICE and ME2 are off. We run the MPC in this mode with the discrete time interval of 0.05 second. ME1 has max power of 35 kW and max torque of 205 Nm, rigidity torque $k_\theta = 1158$, inertia $J_2 = 1$, constants $k_{E2} = k_{T2} = 10$, inertia $J_3 = 2$, gear ratio $i = 2.34$, damping $k_{\beta2} = 0.5$ and $k_{\beta3} = 12$, resistance $R_{I2} = 5$.

Some softened constraints are converted as input constraints for the DC voltage applied for the vehicle is $|V_2| \leq 250V$, $\Delta u(t) \leq +/-5V$. The output softened constraints are also set on the shaft with the shear strength for carbon steel of $\tau = 25$ *MPa* or N/mm². The output torque on the shaft 2 is constrained as $|T| = \tau\pi\frac{d^3}{16}$, where the diameter $d = 0.05m$. Then, the torque softened constraint on shaft 2 is $|T_2| \leq 455Nm$.

The MPC parameters are set up with the predictive horizon of $N_u = N_y = N_p = 5$, the weighting matrices are set at $Q = \begin{bmatrix} 1 & 0 \\ 0 & 1 \end{bmatrix}$ and $R = [1]$. The MPC performance with softened constraints is shown in Figure 6.
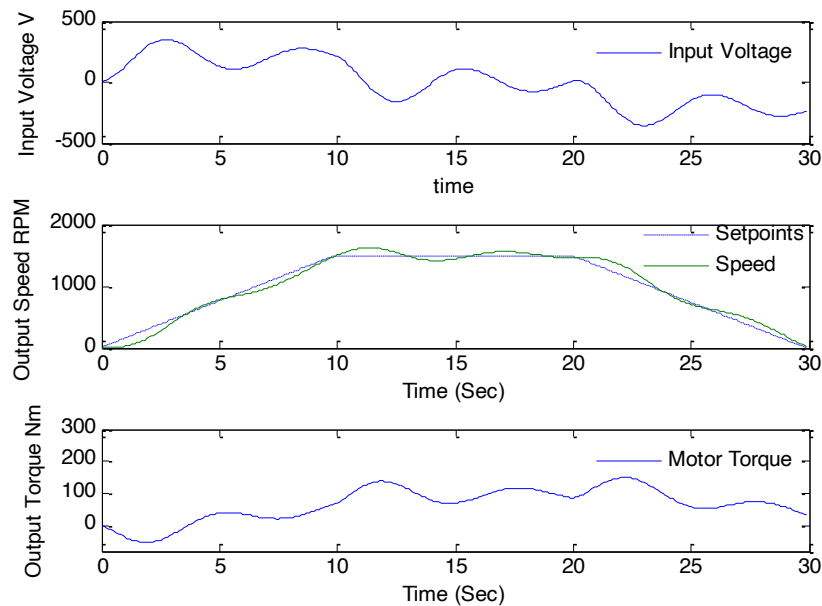

Figure 6. MPC for HEV with $N_p = 5$ and $Q = R$

It is noted that, the weighting matrix for output Q and input R can be varied according to the desired variation on outputs or inputs. If we want to limit the errors or keep the output variation in small value, we have to pay for more input energy or increase the input variation. By this aim, we increase Q and reduce R. It means that any small variation in output will lead to a big penalty amount adding to the MPC objective function. Figure 7 shows the MPC for HEV performance with Q=100 and R=1.
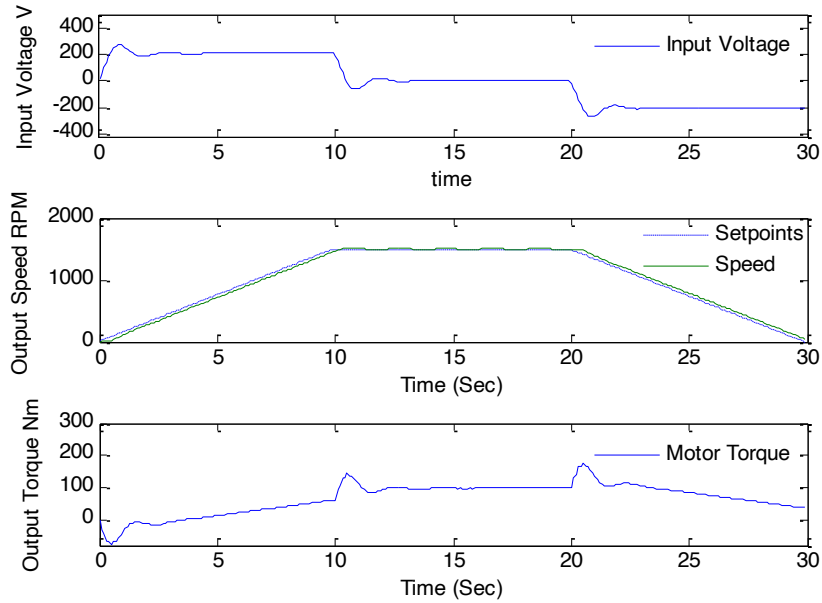
Figure 7. MPC for HEV with $N_p = 5$, Q=100 and R=1

As shown in Figure 6 and Figure 7, we set up softened constraint on the input voltage of $|V_2| \leq 250V$, the MPC allows a little bit input voltage violation at the starting time to insure the controller stability and feasibility. Then, after a very short transitional period, the solution is returned without constraint violation. In these cases, the MPC with hard constraints becomes infeasible and unstable.

5.2 MPC for HEV in high speed with ICE

When the HEV runs in high speed, the starter/generator ME2 starts the ICE. Depending on the required output torque, the ICE alone or the ICE and ME1 or all ICE, ME1 and ME2 will be running and together providing torque.

At this mode, we assume that the vehicle is running at $\omega_3 = 2000$rpm, and the torque of the air drag resistance at this speed of $M_{v0} = 30$ Nm. Parameters of the starter motor EM2 are as constants $k_{E2} = k_{T2} = 15$, inertia $J_1 = 1$, damping coefficient $k_{\beta 1} = 0.5$, resistance $R_{I1} = 7$, compensation $\varsigma = 0.5$, the discrete time of 0.05 second.

The softened constraints are imposed on input voltage constraints for the starter of $|V_1| \leq 48V$, $\Delta u(t) \leq +/-5V/interval$ and the output constrained torque on shaft 1 of $|T_1| \leq 638Nm$.

For the MPC parameters, we select the predictive horizon length of $N_u = N_y = N_p = 5$ and the weighting matrices $Q = \begin{bmatrix} 10 & 0 \\ 0 & 10 \end{bmatrix}$ and $R = \begin{bmatrix} 1 & 0 \\ 0 & 1 \end{bmatrix}$. The MPC performance with starting EM2 is shown in Figure 8.
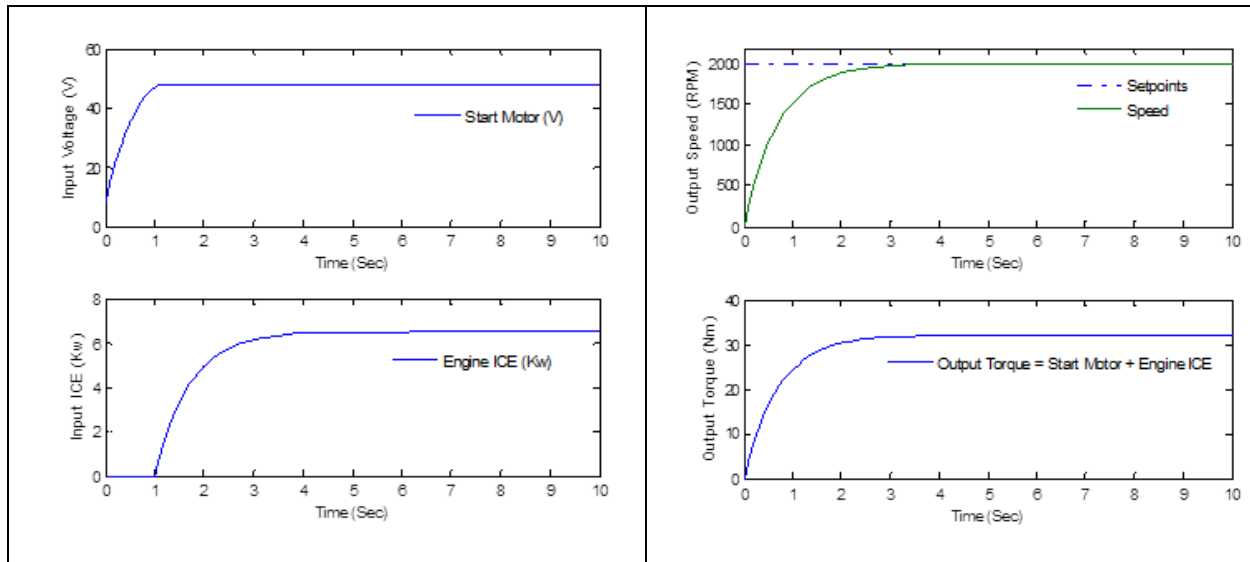
Figure 8. MPC for HEV with ICE and ME2

Figure 8 shows that the EM2 starts in 1 second and the ICE is fully ignited and run in 2.3 seconds, the ICE speed reaches the setpoints of 2000 rpm and steadily run at 6.2 kW providing the output torque of 31 Nm.

In the next simulation, we will run the EM2 and the ICE for tracking the speed desired setpoints and ignite the clutch engagement. It is assumed that the main motor EM1 now running at 1500 rmp and the starter EM2 starts the ICE and engaged into the system. The clutch engagement must be taken place at $\omega_1 \geq \omega_2$ or $\omega_1 = 1.05 * \omega_2$ for the driving comfortability and low jerk. The ICE and ME2 must track on the EM1 speed at +5% offset. The fully engagement is fully done in 2.3 seconds and shown in Figure 9.
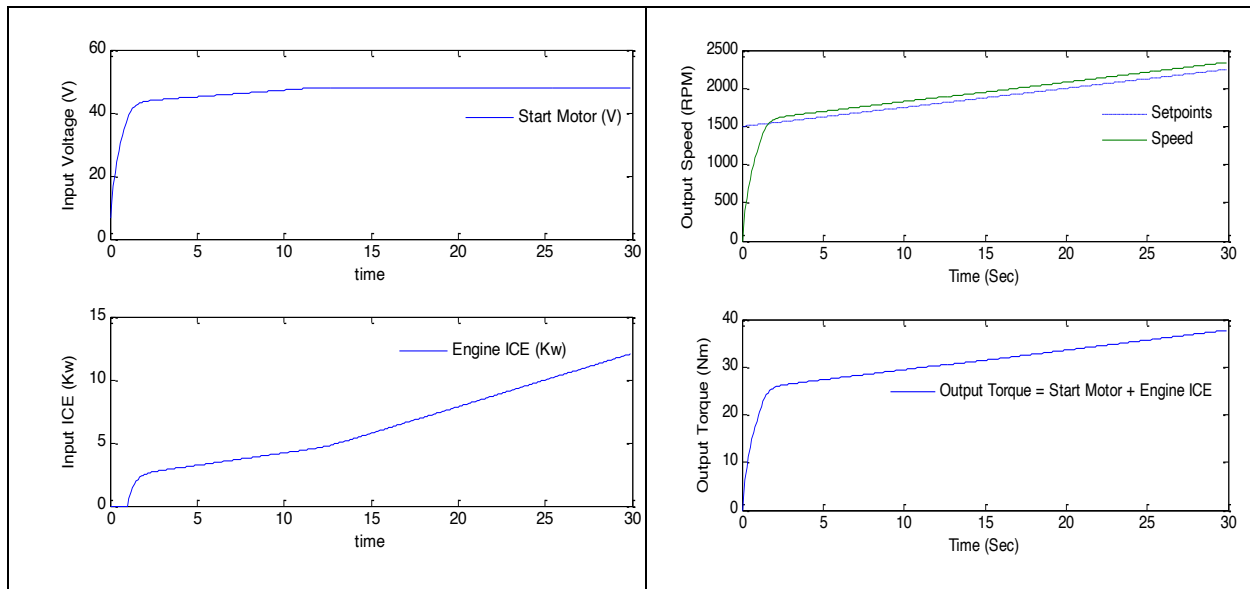

Figure 9. MPC for HEV with ICE and ME2

In Figure 9, we see ICE and ME2 tracking ME1 on desired setpoints in 1.9 seconds. In normal mode at speed higher than 40 km/h, the starter ME2 ignites the ICE and is

turned as a generator charging to battery. The main motor EM1 now is also turned off. Anh only the ICE propels the HEV.

In Figure 10, the ME2 is turned off and becomes the generator after igniting the ICE. The main motor EM1 is also turned off and the ICE alone propels the HEV. The HEV reaches and tracks the desired speed setpoints after 3.5 seconds.
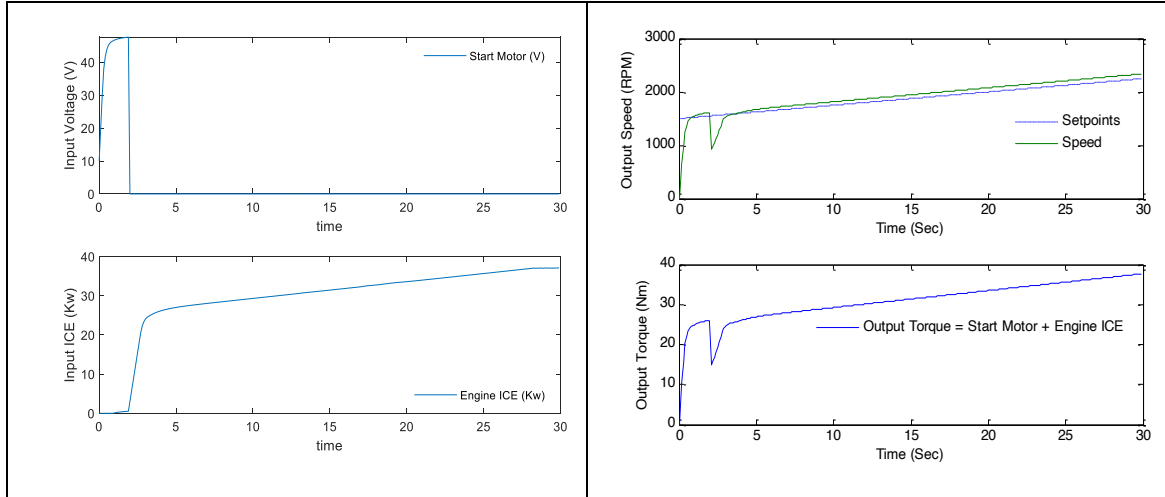

Figure 10. MPC for HEV propelled by only ICE

Finally, we compare the performances of MPC with hard constraints and MPC with softened constraints. We run the MPC with hard constraints in (31) and the MPC with softened constraints in (36) to track the desired speed setpoints in Figure 11.
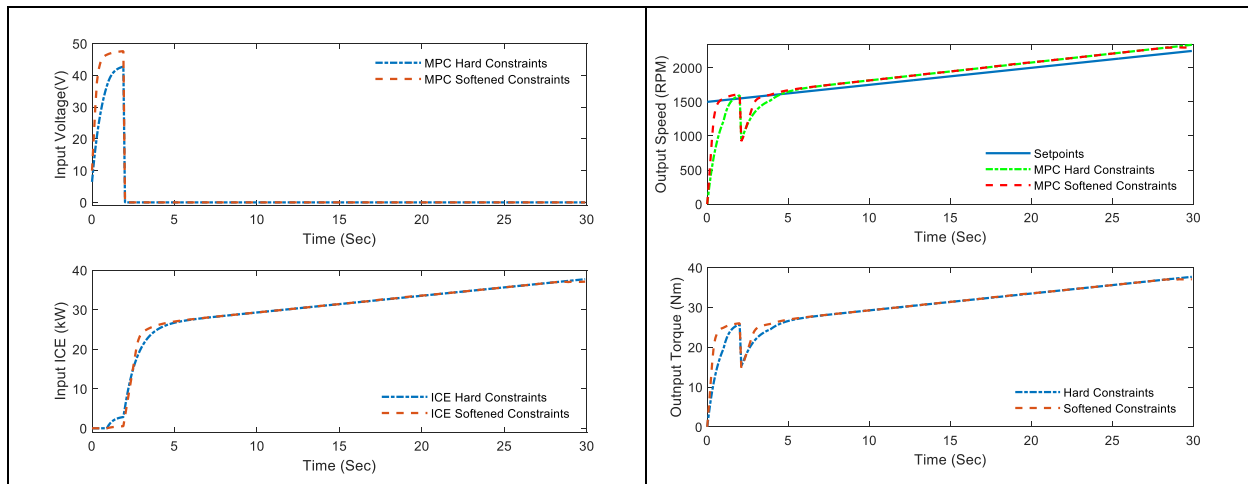

Figure 11. Two MPC performances comparison

Figure 11 shows that the MPC with hard constraints generates smaller inputs and hence needs longer time to track into the speed setpoint. The MPC with hard constraints reaches the speed setpoint after 4.5 seconds while the MPC with softened constraints needs only 3.5 seconds to fully track into the speed setpoint.

6. CONCLUSION

In this study, we have presented the modelling of HEV and the MPC algorithms for controlling HEV. In the HEV modelling, we have included the system acceleration and jerk into equations to investigate and compare the vehicle driving comfortability with different control parameters. The MPC scheme with softened constraints has proved its superiority over the MPC with only hard constraints. The control system now becomes more flexible, stable and robust against model uncertainties, time variant and constraint violations. The new MPC scheme can control the HEV with faster clutch engagement and lower jerk reduction. MPC with softened constraint still stable and robust while the MPC with only hard constraints becomes unstable and infeasible because of the constraint violations. In the next study, we will investigate the control of the HEV friction clutch for smooth and fast engagement with high comfortability and low jerk and apply these algorithms in the real HEV.

CONFLICT OF INTERESTS

The authors would like to declare that there is no conflict of interest regarding the publication of this research article

REFERENCES

[1]   Hyundai Sonata. Available at https://www.hyundaiusa.com/us/en/vehicles/sonata-hybrid. Accessed on 04 October 2022.

[2]   Moustafa A. and Minh, V.T., Modeling and simulation of dual clutch transmission and hybrid electric vehicles, *In: 11th International Conference of DAAAM Baltic Industrial Engineering*, Tallinn, Estonia, 2016; p. 168–174.

[3]   Minh V.T., Moezzi R., Dhoska K. and Pumwa J. Model Predictive Control for Autonomous Vehicle Tracking, *International Journal of Innovative Technology and Interdisciplinary Sciences*, 2021; 4(1); 560-603.

[4]   Mrochen M.A. & Sawodny O. Modeling and Simulation of a Hybrid Dual-Clutch Transmission Powertrain, *IFAC-PapersOnLine*, 2018; 51(31); 886-891.

[5]   Takahashi Y. & Hidaka K. Model Predictive Control for Hybrid Electric Vehicles with Linear Parameter-Varying Model, *In: 2018, 18th International Conference on Control, Automation and Systems (ICCAS)*, PyeongChang, Korea, 2018, p. 1501-1506

[6]   Hua X., Zhanga X., Tanga X. & Lin X. Model predictive control of hybrid electric vehicles for fuel economy, emission reductions, and inter-vehicle safety in car-following scenarios, *Energy*, 2020; 196(1); 1-13.

[7]   Chen Y., Feng G., Wu S. and Tan X. A New Hybrid Model Predictive Controller Design for Adaptive Cruise of Autonomous Electric Vehicles, *Journal of Advanced Transportation*, 2021; 2021; 6626243.

[8]   Glos J., Solc F., Otava L. and Vaclavek P. Hybrid Model Predictive Control for Fully Electric Vehicle Thermal Management System Optimal Mode Selection, *In: IECON 2020 The 46th Annual Conference of the IEEE Industrial Electronics Society*, Singapore, 2020; p. 2036-2043.

[9]   De Mauri M., Gillis J., Swevers J. & Pipeleers G. Real-Time Model Predictive Control for a Parallel Hybrid Electric Vehicle using Outer Approximation and Semi-Convex Cut Generation, *IEEE 16th International Workshop on Advanced Motion Control*, Kristiansand, Norway, 2020; p. 198-203.

[10] Oncken J. and Chen B. Real-Time Model Predictive Powertrain Control for a Connected Plug-In Hybrid Electric Vehicle, *IEEE Transactions on Vehicular Technology*, 2020; 69(8); 8420-8432.

[11] East S. and Cannon M. Scenario Model Predictive Control for Data-based Energy Management in Plug-in Hybrid Electric Vehicles, *IEEE Transactions on Control Systems Technology,* 2022; 30(6); 2522-2533.

[12] Shi D., Wang S., Cai Y., Chen L., Yuan C.C. and Yin C.F. Model Predictive Control for Nonlinear Energy Management of a Power Split Hybrid Electric Vehicle, *Intelligent Automation and Soft Computing*, 2020; 26(1); 27-39.

[13] Zhang F., Hu X.S., Liu T.L., Xu K., Duan Z.D. and Pang H. Computationally Efficient Energy Management for Hybrid Electric Vehicles Using Model Predictive Control and Vehicle-to-Vehicle Communication, *IEEE Transactions on Vehicular Technology*, 2020; 70(1); 237-250.

[14] Torreglosa J.P., Garcia-Triviño P., Vera D. and López-García D.A. Analyzing the Improvements of Energy Management Systems for Hybrid Electric Vehicles Using a Systematic Literature Review: How Far Are These Controls from Rule-Based Controls Used in Commercial Vehicles? *Applied Sciences*, 2020; 10(23); 1-25.

[15] Liu W., Chen G. & Knoll A. Matrix Inequalities Based Robust Model Predictive Control for Vehicle Considering Model Uncertainties, External Disturbances, and Time-Varying Delay, *Frontiers in Neurorobotics*, 2021; 14; 617293.

[16] Schmitt L., Keller M., Albin T. and Abel D. Real-Time Nonlinear Model Predictive Control for the Energy Management of Hybrid Electric Vehicles in a Hierarchical Framework, *2020 American Control Conference*, Denver, USA, 2020; p.1961-1967.

[17] Ibrahim M.H., Maghfiroh H., Nizam M. & Apribowo C.H.B. Plug-in hybrid electric vehicle mode selection strategy for full battery consumption and known road slope condition, AIP *Conference Proceedings*, 2020; 2217; 030149.

[18] Germanà R., Liberati F. & Di Giorgio A. Decentralized Model Predictive Control of Plug-in Electric Vehicles Charging based on the Alternating Direction Method of Multipliers, 2020, *In: 28th Mediterranean Conference on Control and Automation* (MED), September 2020 - Saint-Raphaël, France, 2020; p. 739-745.

[19] Qi Y., Xiang C., Wang W., Wen B. and Ding F., Model Predictive Coordinated Control for Dual Mode Power Split Hybrid Electric Vehicle, *International Journal of Automotive Technology*, 2018; 19(2); 345-358.

[20] Wang Y., Cao S., Yang H., Zuo Z., Wang L. & Luo X. Model predictive longitudinal control for autonomous electric vehicles with tracking differentiator, *International Journal of Systems Science*, 2021; 52(12); 2564-2579.

[21] Liu H., Yan S., Shen Y., Li C., Zhang Y. and Hussain F. Model predictive control system based on direct yaw moment control for 4WID self-steering agriculture vehicle, *International Journal of Agricultural and Biological Engineering*, 2021; 14(2); 175-181.

[22] Zhang B., Xu F., Zhang J. & Shen T. Real-time control algorithm for minimising energy consumption in parallel hybrid electric vehicles, *IET Electrical Systems in Transportation*, 2019; 10(6); 331-340.

[23] Minh V.T. (2012) Advanced Vehicle Dynamics, Publisher: Kuala Lumpur, Universiti of Malaya Press, Malaysia.

[24] Minh V.T. and Afzulpurkar N. Robust model predictive control for input saturated and softened state constraints, *Asian Journal of Control*, 2005; 7(3); 319-325.

[25] Minh V.T. & Mohd Hashim F. Adaptive teleoperation system with neural network-based multiple model control. *Math. Probl. Eng.,* 2010; 2010; 592054.

[26] Minh V.T. and Afzulpurkar N. Robustness of model predictive control for Ill-conditioned distillation process. *Dev. Chem. Eng. Min. Process.* 2005; 13(3-4); 311-316.

[27] Minh V.T., Oamen G, Vassiljeva K and Teder L. Development of Anti-lock Braking System (ABS) for Vehicles Braking. *Open Eng.* 2016; 6(1); 554-559.

[28] Minh V.T., Tamre M., Moezzi R., Oliver M., Martin J., Ahti P., Leo T. and Juurma M. Performances of PID and Different Fuzzy Methods for Controlling a Ball on Beam. *Open Eng.* 2016; 6; 145-151.

[29] Minh V.T. and Rashid A.A. Automatic control of clutches and simulations for parallel hybrid vehicles, *International Journal of Automotive Technology*, 2012; 13; 645-651.

[30] Minh V.T. & Hashim F.B.M. Tracking setpoint robust model predictive control for input saturated and softened state constraints, *International Journal of Control, Automation and Systems,* 2011; 9(5); 958-965.

[31] Minh V.T. Conditions for stabilizability of linear switched systems. *AIP Conference Proceedings,* 2011; 1337(1); 108-112.

[32] Minh V.T. (2014). Trajectory Generation for autonomous vehicles, In: Březina, T., Jabloński, R. (eds) Mechatronics 2013. Springer, Cham. https://doi.org/10.1007/978-3-319-02294-9_78.